

Model for Photoresponsive Nematic Elastomers

André M. Sonnet^{1*} and Epifanio G. Virga^{2*†}

^{1*}Department of Mathematics and Statistics, University of Strathclyde, 26 Richmond Street, Glasgow, G1 1XH, U.K..

^{2*}Dipartimento di Matematica, Università di Pavia, Via Ferrata 5, Pavia, 27100, Italy.

*Corresponding author(s). E-mail(s): andre.sonnet@strath.ac.uk; eg.virga@unipv.it;

†These authors contributed equally to this work.

Abstract

We study the equilibria of a photoresponsive nematic elastomer ribbon within a continuum theory that builds upon the statistical mechanics model put forward by Corbett and Warner [Phys. Rev. E **78**, 061701 (2008)]. We prove that the spontaneous deformation induced by illumination is *not* monotonically dependent on the intensity I . The ribbon's deflection first increases with increasing I , as expected, but then decreases and abruptly ceases altogether at a critical value I_e of I . I_e , which is enclosed within a hysteresis loop, marks a first-order *shape transition*. Finally, we find that there is a critical value of the ribbon's length, depending only on the degree of cross-linking in the material, below which *no* deflection can be induced in the ribbon, no matter how intense is the light shone on it.

Keywords: Photoresponsive elastomers, Nematic liquid crystals, Shape transition, Ribbon elasticity.

MSC Classification: 74B20 , 74K10 , 74K35 , 76A15 , 82D30

1 Introduction

Nematic elastomers are elastic materials comprising cross-linked polymer networks made of nematogenic, rod-like molecules which at sufficiently low temperatures develop a collective orientational order. Despite polymer strands being cross-linked, the constituting monomers are quite loose; they are the fluid component of a mixture whose other component is a solid-like matrix kept together by the cross-linking bonds [1].

These materials can be *reversibly* activated by changing the temperature across the nematic-isotropic transition. Upon increasing the temperature, the nematic order is decreased, the fluid becomes isotropic and the larger availability of orientational states produces a mechanical contraction of the solid matrix along the nematic director designating the pre-existing average molecular orientation. Conversely, decreasing the temperature across the nematic-isotropic transition, an elongation takes place along the newly reconstituted nematic director, as molecules would tend to be mostly oriented in that direction. This is perhaps the most remarkable mechanical property of nematic liquid crystal elastomers (LCEs): they can undergo a shape change of up to 400% in a relatively narrow temperature range (including the nematic-isotropic transition of the fluid component).

Such a thermal activation mechanism was the only one known and studied until the groundbreaking work [2] was published in 2001. That paper explored a new possible avenue for mechanical activation of nematic LCEs: using light instead of heat. The idea was simple: if a macroscopic change in shape is caused by a change in molecular order, the latter should result in the former, whatever means are employed. Now, order can either be decreased by raising the temperature or by disturbing molecules otherwise, making it harder for them to be oriented alike.

Since the pioneering work of Eisenbach [3], this could be achieved by dispersing in the material photoisomerizable molecules, such as azobenzene and other dyes, which undergo a *trans-cis* isomerization upon absorbing a photon of appropriate frequency. These molecules, which are typically rod-like in the *trans*-state, become bent in the *cis*-state. Such a change in shape has a disrupting effect on surrounding molecules in the nematic phase, which remain straight, decreasing their degree of order (as first shown in [4]).¹ The specific situation envisioned in this paper is illustrated in Fig. 1, which also shows dye molecules in both *trans*- and *cis*-states.

Such a disruption of the nematic order is reversible. Photoresponsive molecules do not stay indefinitely in the *cis*-state; this, although locally stable, has greater energy than the *trans*-state, and thermal relaxation suffices to overcome the energy barrier that prevents excited molecules to drop to the *trans*-state right away. Once photoresponsive molecules are back in the *trans*-state, their reacquired rod-like shape no longer contrasts the alignment of

¹Similar effects could also be imparted on the director \mathbf{n} , but they will be ignored in this paper, as here \mathbf{n} will be enslaved to the macroscopic deformation, an assumption which will be further discussed and justified below.

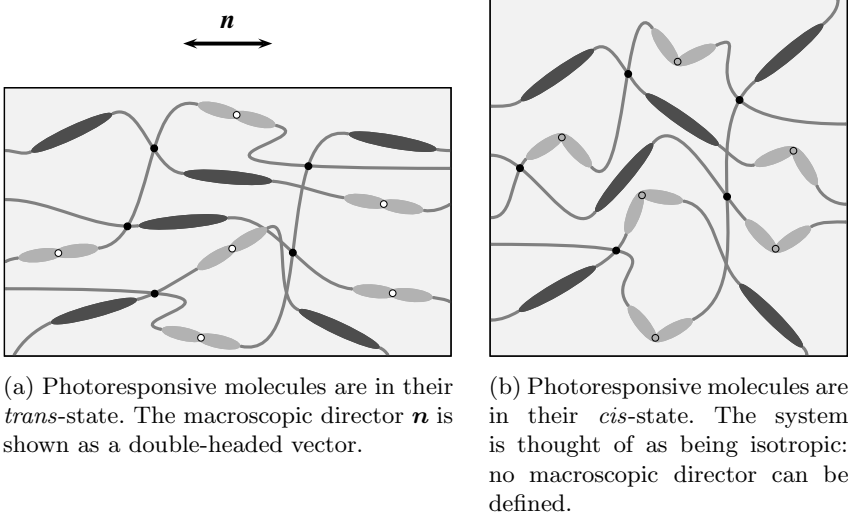


Fig. 1: Cartoons illustrating the photoactivation of isomerizable molecules. They are straight in their *trans*-state and bent in their *cis*-state. Forward activation is induced by a photon absorption; backward relaxation is induced by thermal agitation, with no change in temperature involved. In our model, photoresponsive molecules are part of the polymer chains, within which, upon activation, they deplete nematic order. The case envisioned here is listed as case (ii) in the text.

monomers in the polymer strands, and nematic order can be reinstated. Thus, with no change in temperature, a change in order induced by light can produce a typical thermo-mechanical effect.

There are at least three possibilities for a photoisomerizable molecule to play its actuating role within a nematic elastomer network: (i) by being freely dispersed through it, (ii) by being part of the network itself, linked at a polymer chain at both its ends, (iii) by being linked to a polymer chain side-wise at an end, with the other end dangling freely. They may all be effective.

Here, we shall consider case (ii): for simplicity, we shall further assume that when photoresponsive molecules are in the *trans*-state they have the same length a as the photoinert nematic monomers in the polymer strands. In their *trans*-state, photoresponsive molecules are indistinguishable from nematogenic molecules, they obey the same statistics (see Fig. 1a). Light activation induces the *trans-cis* transition and changes the distance between the ends of the two arms of photoresponsive molecules (see Fig. 1b) from a to $b < a$. This transition causes a depletion in the population of rods obeying nematic statistics and a repletion in the population of isotropically distributed rods: as such we regard photoresponsive molecules in the *cis*-state.

The stationary equilibrium between the light-induced *trans-cis* transition and its reverse thermal relaxation determines the fraction ϕ of the

cis-population in terms of the nematic scalar order parameter S and the orientation of the nematic director \mathbf{n} relative to the wave polarization unit vector \mathbf{e} [5, 6]. Both ϕ and S in turn affect the *step tensor* \mathbf{L} describing the distribution of chain elements in a representation of polymer strands as freely jointed rigid rods.

The intricate interplay between these microscopic processes is described by the model recalled in Sect. 2. This model is originally due to Corbett and Warner [5–7] (see also [1, 8]).

In Sect. 3, we build the macroscopic theory that we shall adopt here. Its main ingredient is the celebrated *trace formula* for the elastic free-energy density (per unit volume) of nematic LCEs that has long been studied [9–12] (see also Chap. 6 of [13]).

As effectively recalled in [14], nematic LCEs have also come to be known in the specialized literature under a variety of names, including liquid crystal polymers, cross-linked liquid crystal polymers, and liquid crystal polymer networks. What marks the difference between these names is their different range of applicability, which is essentially decided by the extent of cross-linking: the higher this is, the stiffer the material becomes and the more is the nematic director \mathbf{n} linked to the polymer matrix. When \mathbf{n} is completely enslaved to the macroscopic deformation, which is the case of extreme cross-linking, also the name *nematic polymer network* (NPN) is used for these materials.²

It has recently become clear [16] that the mechanical response changes continuously with the extent of cross-linking. To fix ideas, we find at the NPN end of the spectrum a transition temperature ranging from 60 to 100 °C with shear modulus parallel to the nematic director in the range of 1–2 GPa. At the opposite end of the spectrum transition temperatures are below 25 °C with shear moduli about 100 MPa or lower [14].

Since in our model the scalar order parameter S is *not* the driving parameter of spontaneous deformation, as the temperature is kept fixed, a further potential must supplement the trace formula, which penalizes departures from the equilibrium value S_0 of S , which is dictated by temperature. This role will be played here (as was in [18]) by the Maier-Saupe potential [17].

In Sect. 3, we shall also adapt to the present setting the surface elastic free energy density (per unit area) obtained in [19] for a thin NPN sheet by extending a method of dimension reduction, which is standard in the theory of plates and also known as the Kirchhoff-Love hypothesis [20]. This surface free energy features both stretching and bending contributions, which here are reformulated in the language of the model illustrated in Sect. 2.

In Sect. 4, we apply the reduced elastic free energy for a sheet to a narrow ribbon and study its equilibrium configurations in terms of a dimensionless intensity parameter I . Resorting to a uniformity approximation, we simplify the total free-energy functional for a ribbon to an extent that makes it possible to find its critical points in closed form. The bifurcation analysis that ensues

²As well as nematic *glass*, as for example in [15].

reveals a non-monotonic dependence on I of the maximum deflection angle of an illuminated ribbon.

Our conclusions are collected and discussed in Sect. 5 together with comparisons of our work with that of others. The paper is closed by an Appendix, where for completeness we recall the reasoning that is followed in [7] to justify both the equilibrium value ϕ of the *cis*-population and the expressions for the principal chain steps (i.e., the eigenvalues of \mathbf{L}) after photoactivation.

A vast, nearly intimidating literature is available on nematic LCEs. The classical reference is the influential book by Warner and Terentjev [13]; the theoretical literature that preceded and prepared for it [9, 21–25] is also of interest. General continuum theories have also been proposed [26–28], some also very recently. Applications are abundant; a collection can be found in a book [29] and a recent special issue [30]. Finally, the interested reader can gain some valuable guidance from the reviews [31–37].

The specific theme of this paper is photoactivation of NPN sheets; the recent studies [18, 38, 39] are closely related to it and, notwithstanding the differences, they have been inspirational to us.

2 The Corbett-Warner Model

In this section, mainly following [5–7], we present a statistical mechanics model put forward by Corbett and Warner to describe the interaction of an incoming polarized light wave with a nematic elastomer containing photoactivable molecules in its polymer strands, as depicted in Fig. 1. For completeness, the reasoning that led these authors to their understanding of shape effects induced on polymer networks by the *trans-cis* transition is described in more detail in Appendix A. Here, our main focus is on the foundations of the model and its main outcomes, which will form the basis for our macroscopic theory laid down in the following section.

The model is based on the following assumptions:

1. Photoresponsive molecules in their *trans*-state and photoinert (non-photoresponsive) molecules are assumed to be *statistically* identical.
2. Photoresponsive molecules in the *cis*-state are statistically *isotropic*.
3. The forward *trans-cis* photoisomerization is powered by light, whereas the backward *cis-trans* transition is spontaneously driven by thermal agitation.
4. The *trans-cis* reaction is treated at the *single-molecule* level: equilibrium at one molecule is not affected by its interaction with surrounding molecules.

Polymer strands, constituted of both photoresponsive and photoinert molecules, are represented as chains of freely jointed rigid rods; the orientation in space of an individual rod will be represented by a unit vector $\mathbf{u} \in \mathbb{S}^2$. The

order tensor \mathbf{Q} describing the alignment of mesogenic monomers is defined as

$$\mathbf{Q} := \left\langle \mathbf{u} \otimes \mathbf{u} - \frac{1}{3} \mathbf{I} \right\rangle, \quad (1)$$

where \mathbf{I} is the identity tensor and the brackets $\langle \dots \rangle$ designate ensemble averaging. We shall assume that \mathbf{Q} is *uniaxial*, and so it can be represented as

$$\mathbf{Q} = S \left(\mathbf{n} \otimes \mathbf{n} - \frac{1}{3} \mathbf{I} \right), \quad (2)$$

where S is the *scalar* order parameter, ranging in the interval $[-\frac{1}{2}, 1]$, and $\mathbf{n} \in \mathbb{S}^2$ is the nematic *director*.³ It readily follows from (2) that

$$S = \langle P_2(\mathbf{u} \cdot \mathbf{n}) \rangle, \quad (3)$$

where P_2 is the second Legendre polynomial.

In the following, S and \mathbf{n} will represent the scalar order parameter and the nematic director in the *present* (photoactivated) configuration of the material, after the spontaneous deformation of the body induced by illumination has taken place. Since we also assume that prior to photoactivation the polymer system had been cross-linked in the nematic phase, we shall denote by S_0 and \mathbf{n}_0 the scalar order parameter and the nematic director in the *reference* configuration, prior to illumination. \mathbf{Q}_0 , related to S_0 and \mathbf{n}_0 as \mathbf{Q} is to S and \mathbf{n} in (2), will denote the corresponding order tensor.

The nematic order in the material is also reflected by the *step tensor*, which describes the spatial organization of polymer strands (see Appendix A.1 for a formal definition). Since there are two different polymer organizations, in the reference and present configurations, there will correspondingly be two step tensors, \mathbf{L}_0 and \mathbf{L} . They have the same uniaxial form as \mathbf{Q}_0 and \mathbf{Q} , respectively, and are represented as

$$\mathbf{L}_0 = \ell_{0\perp} \mathbf{I} + (\ell_{0\parallel} - \ell_{0\perp}) \mathbf{n}_0 \otimes \mathbf{n}_0, \quad (4a)$$

$$\mathbf{L} = \ell_{\perp} \mathbf{I} + (\ell_{\parallel} - \ell_{\perp}) \mathbf{n} \otimes \mathbf{n}, \quad (4b)$$

where $(\ell_{0\perp}, \ell_{0\parallel})$ and $(\ell_{\perp}, \ell_{\parallel})$ are the corresponding *principal chain steps* in the directions orthogonal and parallel to the directors \mathbf{n}_0 and \mathbf{n} (see Appendix A.1).

The principal chain steps $(\ell_{0\perp}, \ell_{0\parallel})$ in the reference configuration are related to the scalar order parameter S_0 in the following way,

$$\ell_{0\perp} = a(1 - S_0), \quad \ell_{0\parallel} = a(1 + 2S_0), \quad (5)$$

³ \mathbf{Q} is the deviatoric part of the second-moment distribution of monomer \mathbf{u} 's: $S = -\frac{1}{2}$ when all \mathbf{u} 's are uniformly distributed in the plane orthogonal to \mathbf{n} , while $S = 1$ when all \mathbf{u} 's are aligned with \mathbf{n} , and $S = 0$ when all \mathbf{u} 's are isotropically distributed (and \mathbf{n} is undefined), see, for example, Chapt. 1 of [40].

where a is the *step length* that both photoinert nematogenic molecules and photoresponsive ones in the *trans* configuration are assumed to have in common.

A statistical mechanics argument of Corbett and Warner [5, 6] justifies writing the principal chain steps $(\ell_\perp, \ell_\parallel)$ in the present configuration as

$$\ell_\perp = a \left[(1 - \phi)(1 - S) + \phi \left(\frac{b}{a} \right)^2 \right], \quad \ell_\parallel = a \left[(1 - \phi)(1 + 2S) + \phi \left(\frac{b}{a} \right)^2 \right], \quad (6)$$

where S is the scalar order parameter after photoactivation, $b < a$ is the step length of photoresponsive nematogens in the *cis* configuration, and ϕ is the *number fraction* of these molecules (see Appendix A.1). It should be noted that for $\phi = 0$ equation (6) reduces to (5), only with S instead of S_0 .

The equilibrium value of ϕ depends on how light impinges on the material. Letting the unit vector $\mathbf{e} \in \mathbb{S}^2$ denote the polarization of the incoming light, that is, the direction of vibration of the electric field, it was shown in [6] that in equilibrium

$$\phi = A \frac{\mathcal{I}[1 + S(3(\mathbf{n} \cdot \mathbf{e})^2 - 1)]}{3\mathcal{I}_c + \mathcal{I}[1 + S(3(\mathbf{n} \cdot \mathbf{e})^2 - 1)]}, \quad (7)$$

where A is the fraction of photoresponsive nematogens in a polymer strand, \mathcal{I} is the intensity of light, and \mathcal{I}_c a characteristic intensity, related to both forward and reverse isomerization rates (see Appendix A.2).

For unpolarized light, which is the case that we shall consider in this paper, $(\mathbf{n} \cdot \mathbf{e})^2$ should be replaced in (7) by its average over a uniform distribution of \mathbf{e} in the unit circle $\mathbb{S}_\mathbf{k}^1$ lying in the plane orthogonal to the unit vector $\mathbf{k} \in \mathbb{S}^2$ designating the direction of propagation of light. Since

$$\langle (\mathbf{n} \cdot \mathbf{e})^2 \rangle_{\mathbb{S}_\mathbf{k}^1} = \mathbf{n} \cdot \langle \mathbf{e} \otimes \mathbf{e} \rangle_{\mathbb{S}_\mathbf{k}^1} \mathbf{n} = \mathbf{n} \cdot \frac{1}{2} (\mathbf{I} - \mathbf{k} \otimes \mathbf{k}) \mathbf{n} = \frac{1}{2} (1 - (\mathbf{n} \cdot \mathbf{k})^2), \quad (8)$$

equation (7) will be replaced here by

$$\phi = A \frac{\mathcal{I} \left[1 + \frac{S}{2} (1 - 3(\mathbf{n} \cdot \mathbf{k})^2) \right]}{3 + \mathcal{I} \left[1 + \frac{S}{2} (1 - 3(\mathbf{n} \cdot \mathbf{k})^2) \right]}, \quad (9)$$

where

$$I := \frac{\mathcal{I}}{\mathcal{I}_c} \quad (10)$$

is the *relative* intensity, a dimensionless quantity that in our analysis will play the role of a *control* parameter.

It is a simple matter to check that for $S < 1$ the function delivering ϕ in (9) tends to the asymptotic value A for $I \rightarrow \infty$ (the bleaching limit). Moreover, letting ϑ be the angle that \mathbf{k} makes with \mathbf{n} , for a given intensity I , ϕ is either a monotonic increasing or decreasing function of ϑ for either $S > 0$ or $S < 0$, respectively. Thus, for positive S , the photoactivation mechanism described

above is most efficient when \mathbf{n} and \mathbf{k} are at right angles. If a deformation of the body moves \mathbf{n} closer to \mathbf{k} , at a given intensity, photoactivation may be weakened.

In general, light is absorbed in a material, in a way that depends on the penetration depth and direction of propagation of the radiation, as described, for example, by Beer's law [41] (see also Chapt. 1 of [42]). Here, this classical picture is further complicated by the fact that absorption also depends on the population of photoresponsive molecules in the *trans*-state, but not on those in the *cis*-state. To account properly for this would require coupling the population evolution equation resulting in (7) at equilibrium with an attenuation equation for the intensity, as proposed in [8].

Here, we shall only be concerned with thin films, and we shall make the approximation that the intensity of light remains unaffected through the thickness of the body. We shall refer to this as the *photo-uniformity* approximation. Of course, this will have a price: we shall not be able to capture the symmetry breaking associated with the direction of propagation of light. Whatever instability we shall be able to predict with our continuum theory, flipping *towards* or *away* from light, such as in the experiments described in [43], [44], or [45], will come from extrinsic *ad hoc* considerations. We shall be contented with capturing exactly (possibly in a closed form) just the *flipping* (in either direction), if any.

3 Free-Energy Functional

Our continuum theory is based on the *trace formula* for the elastic free energy per unit volume (in the reference configuration) of nematic LCEs in the form put forward in [46],

$$f_e = \frac{1}{2}\mu_0 \left\{ \text{tr}(\mathbf{F}\mathbf{L}_0\mathbf{F}^\top\mathbf{L}^{-1}) + \ln \left(\frac{\det \mathbf{L}}{\det \mathbf{L}_0} \right) \right\}, \quad (11)$$

where \mathbf{F} is the deformation gradient and the *shear* elastic modulus μ_0 is given by

$$\mu_0 = n_s k_B T, \quad (12)$$

in terms of the number density of polymer strands n_s , the Boltzmann constant k_B , and the absolute temperature T .

Equation (11) is the nematic generalization of the classical elastic energy density for elastomers, which Rivlin [47] called *neo-Hookian* (see also [48] and the detailed account in Sect. 95 of [49], which sets this constitutive law within the larger class of *Mooney-Rivlin* materials),

$$f_0 := \frac{1}{2}\mu_0 \text{tr} \mathbf{C}_f, \quad (13)$$

where $\mathbf{C}_f := \mathbf{F}^\top \mathbf{F}$ is the (three-dimensional) right Cauchy-Green tensor associated with a deformation \mathbf{f} . A statistical mechanics justification has also been derived for (13) from various theories of long chain molecules.⁴

The function in (11) is obtained by adapting the simplest realization of these theories [51] to the case where in both the reference and present configurations the distribution of monomers in a polymer chain is anisotropic.

When the principal chain steps $(\ell_{0\perp}, \ell_{0\parallel})$ and $(\ell_\perp, \ell_\parallel)$ in both the reference and present configurations are prescribed, as is the case where the corresponding scalar order parameters S_0 and S are given as functions of temperature,⁵ the second term in (11) is not affected by the deformation and can be omitted, thus reducing (11) to the *bare* trace formula of [9] (also discussed in [53]), which depends only on \mathbf{F} and \mathbf{n} .⁶

Our theory will be based on two further assumptions:

- (a) We assume that the director \mathbf{n} is *enslaved* to the deformation, so that

$$\mathbf{n} = \frac{\mathbf{F}\mathbf{n}_0}{|\mathbf{F}\mathbf{n}_0|}, \quad (14)$$

which says that the nematic director \mathbf{n}_0 imprinted in the polymer network at the cross-linking time is *conveyed* by the solid matrix of the body.

- (b) We assume that the material is *incompressible*, so that \mathbf{F} is subject to the constraint

$$\det \mathbf{F} = 1. \quad (15)$$

Clearly, assumption (a) is expected to be more realistic for *strongly* cross-linked polymers than for *weakly* cross-linked ones.⁷ In real life, NPNs (or glassy nematics) are good examples of the former category, as are ordinary nematic LCEs of the latter. On the other hand, while ordinary nematic LCEs have Poisson ratio ν close to 1/2, and so they are nearly incompressible, NPNs may have $\nu \in (1/2, 2)$ [37, 54].

The above assumptions will simplify our analysis a great deal, making tractable the nonlinear problem discussed in the next section. We believe that our model is most appropriate for NPNs and that the conclusions reached here for these materials remain qualitatively valid, should either (14) or (15) be partly relaxed, for example, by means of a penalizing potential.⁸

⁴An exposition of statistical theories for rubber can be found in the landmark book [50].

⁵No photoactivation takes place in this case and a spontaneous deformation of the body is induced by a change in temperature, as recently considered, for example, in [19, 52] and in many other studies reviewed in [37].

⁶An alternative theory building on the bare trace formula is presented in [28], where the existence of an isotropic reference configuration plays a central role.

⁷We shall see shortly below how this difference is accounted for by the choice of a dimensionless model parameter.

⁸However, relaxing (14) completely might ignite pattern formation at a fine scale (such as those studied in [18]), which might change the overall picture.

It is a matter of laborious, but simple algebra, also making use of (14) and (4), to give f_e in (11) the following form

$$f_e = \frac{1}{2}\mu_0 \left\{ \frac{\ell_{0\perp}}{\ell_\perp} \text{tr } \mathbf{C}_f + \frac{1}{\ell_\parallel} (\ell_{0\parallel} - \ell_{0\perp}) \mathbf{n}_0 \cdot \mathbf{C}_f \mathbf{n}_0 \right. \\ \left. + \ell_{0\perp} \left(\frac{1}{\ell_\parallel} - \frac{1}{\ell_\perp} \right) \frac{\mathbf{n}_0 \cdot \mathbf{C}_f^2 \mathbf{n}_0}{\mathbf{n}_0 \cdot \mathbf{C}_f \mathbf{n}_0} + \ln \frac{\ell_\parallel}{\ell_{0\parallel}} + 2 \ln \frac{\ell_\perp}{\ell_{0\perp}} \right\}. \quad (16)$$

In our model, the scalar order parameter S is not prescribed, but is free to adjust itself in response to illumination. The elastic free energy must then be supplemented by the bulk condensation energy for the nematic component. Here we depart from [46]. While they adopted the Landau-deGennes phenomenological approach, we derive the appropriate condensation potential f_c (per unit volume) from the Maier-Saupe mean-field formulation of nematic condensation (from the isotropic phase), as described in Sect. 1.3 of [55]. We set

$$f_c = n_n k_B T (1 - \phi) \psi_{\text{MS}}(S), \quad (17)$$

where n_n is the number density of nematogenic molecules, here appropriately *reduced* to account for their fraction in the *cis*-state (which are no longer in the nematic phase), and

$$\psi_{\text{MS}}(S) := J \left(\frac{1}{3} S^2 - \frac{2}{3} S \right) - \ln \left(\frac{\text{daw}(\sqrt{JS})}{\sqrt{JS}} \right). \quad (18)$$

In (18), J is the Maier-Saupe molecular *interaction energy* (scaled to $k_B T$) and daw denotes the Dawson integral, defined as

$$\text{daw}(x) := e^{-x^2} \int_0^x e^{t^2} dt \quad \text{for } x \in \mathbb{R}. \quad (19)$$

The minimizer of ψ_{MS} depends only on J , which will be chosen so that ψ_{MS} attains its minimum at $S = S_0$, the scalar order parameter prior to illumination.

Scaling the total energy density $f_t := f_e + f_c$ to $n_n k_B T$ (so as to make it dimensionless), we arrive at

$$f_t = \frac{1}{2} \left\{ \mu \left[\frac{\ell_{0\perp}}{\ell_\perp} \text{tr } \mathbf{C}_f + \frac{1}{\ell_\parallel} (\ell_{0\parallel} - \ell_{0\perp}) \mathbf{n}_0 \cdot \mathbf{C}_f \mathbf{n}_0 \right. \right. \\ \left. \left. + \ell_{0\perp} \left(\frac{1}{\ell_\parallel} - \frac{1}{\ell_\perp} \right) \frac{\mathbf{n}_0 \cdot \mathbf{C}_f^2 \mathbf{n}_0}{\mathbf{n}_0 \cdot \mathbf{C}_f \mathbf{n}_0} + \ln \frac{\ell_\parallel}{\ell_{0\parallel}} + 2 \ln \frac{\ell_\perp}{\ell_{0\perp}} \right] \right. \\ \left. + 2(1 - \phi) \psi_{\text{MS}}(S) \right\}, \quad (20)$$

where

$$\mu := \frac{n_s}{n_n} \quad (21)$$

is the *reduced* shear modulus. It is precisely the value of μ that describes in our model the degree of cross-linking in the material: the larger μ , the stronger the cross-linking. Here, following [6], we shall identify two values of μ as representatives for two alternative regimes: $\mu = 1/10$, for *strongly* cross-linked polymers, and $\mu = 1/50$, for *weakly* cross-linked ones.

3.1 Dimension reduction

To treat (in the following section) the equilibrium of a thin sheet, we must first perform an appropriate reduction of the total free-energy density f_t (per unit volume) in (20) to a surface free-energy (per unit area) to be attributed to a surface in three-dimensional space representing the deformed shape of the sheet.

We accomplish this task following mainly [19].⁹ We perform an expansion of f_t retaining up to the cubic terms in the sheet's thickness, thus identifying *stretching* and *bending* contents in the surface energy by the power in the thickness they scale with.¹⁰

We identify the undeformed body with a slab S of thickness $2h$ and mid-surface \mathcal{S}_0 in the $(\mathbf{e}_1, \mathbf{e}_2)$ plane of a Cartesian frame. We further assume that \mathbf{n}_0 is imprinted in S so that it does not depend on the x_3 coordinate and $\mathbf{n}_0 \cdot \mathbf{e}_3 \equiv 0$. Moreover, we represent the three-dimensional deformation \mathbf{f} as

$$\mathbf{f}(\mathbf{x}, x_3) = \mathbf{y}(\mathbf{x}) + \Phi(\mathbf{x}, x_3)\boldsymbol{\nu}, \quad (22)$$

where \mathbf{x} varies in \mathcal{S}_0 , x_3 ranges in the interval $[-h, h]$, $\boldsymbol{\nu}$ is the normal to the midsurface $\mathcal{S} = \mathbf{y}(\mathcal{S}_0)$ of the deformed slab $\mathbf{f}(S)$ (see Fig. 2), and $\Phi(\mathbf{x}, x_3)$ is a function to be determined,¹¹ enjoying the property

$$\Phi(\mathbf{x}, 0) = 0. \quad (23)$$

As shown in [19], the constraint of incompressibility (15) determines Φ in the form

$$\Phi(\mathbf{x}, x_3) = x_3 - Hx_3^2 + \frac{1}{3}(6H^2 - K)x_3^3 + O(x_3^4), \quad (24)$$

where H and K are the *mean* and *Gaussian* curvature of \mathcal{S} , respectively, defined as

$$H(\mathbf{y}(\mathbf{x})) := \frac{1}{2} \text{tr}(\nabla_s \boldsymbol{\nu}) \quad \text{and} \quad K(\mathbf{y}(\mathbf{x})) := \det(\nabla_s \boldsymbol{\nu}), \quad (25)$$

⁹See also [52] for the specific case of a thermally activated ribbon, which differs from the optically activated one studied in the following section.

¹⁰The reader is referred to [56] for an alternative theory for nematic elastomer plates.

¹¹In the classical theory of plates, the *Kirchhoff-Love* hypothesis stipulates that $\Phi \equiv x_3$ (see, for example, [57], for a modern treatment). In [20], the Kirchhoff-Love hypothesis was reformulated in the more general form adopted here and criteria were suggested to identify the function Φ , none of which delivered exactly the original Kirchhoff-Love form.

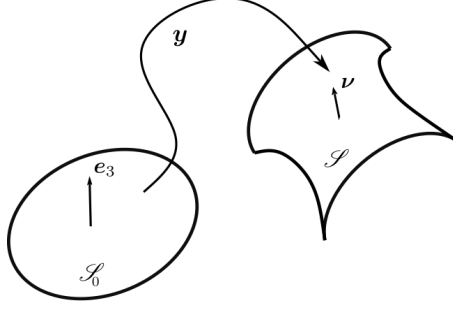


Fig. 2: Schematic representation of the deformation of a thin sheet. \mathcal{S}_0 is the planar midsurface of the slab \mathbf{S} of thickness $2h$ representing the reference configuration of the body. \mathcal{S} is the midsurface of the deformed slab $\mathbf{f}(\mathbf{S})$. \mathcal{S}_0 lies in the plane $(\mathbf{e}_1, \mathbf{e}_2)$ of Cartesian frame $(\mathbf{e}_1, \mathbf{e}_2, \mathbf{e}_3)$. \mathcal{S} is the image under the mapping \mathbf{y} of \mathcal{S}_0 ; it is an oriented surface with unit normal $\boldsymbol{\nu}$.

in terms of the two-dimensional curvature tensor $\nabla_s \boldsymbol{\nu}$ at the point $\mathbf{y}(\mathbf{x})$ on \mathcal{S} . The following formula for \mathbf{F} was justified in [19] as a consequence of (23) for h sufficiently small,

$$\mathbf{F} = \nabla \mathbf{y} + \Phi \nabla \boldsymbol{\nu} + \Phi' \boldsymbol{\nu} \otimes \mathbf{e}_3, \quad (26)$$

where Φ' denotes the derivative of Φ with respect to x_3 and ∇ is the gradient in \mathbf{x} , so that, in particular,

$$\nabla \boldsymbol{\nu} = (\nabla_s \boldsymbol{\nu})(\nabla \mathbf{y}). \quad (27)$$

Since $\mathbf{n}_0 \cdot \mathbf{e}_3 \equiv 0$, it follows from (26) and (14) that the nematic director \mathbf{n} in the present configuration $\mathbf{f}(\mathbf{S})$ is delivered by

$$\mathbf{n}(\mathbf{f}(\mathbf{x}, x_3)) = \frac{(\mathbf{I} + \Phi \nabla_s \boldsymbol{\nu})(\nabla \mathbf{y}) \mathbf{n}_0}{|(\mathbf{I} + \Phi \nabla_s \boldsymbol{\nu})(\nabla \mathbf{y}) \mathbf{n}_0|}, \quad (28)$$

where (27) has also been used. Since $(\nabla \mathbf{y}) \mathbf{n}_0 \cdot \boldsymbol{\nu} \equiv 0$ and $\nabla_s \boldsymbol{\nu}$ is a symmetric tensor mapping the local tangent plane to \mathcal{S} into itself, (28) shows that $\mathbf{n} \cdot \boldsymbol{\nu} = 0$ everywhere within $\mathbf{f}(\mathbf{S})$, but \mathbf{n} is *not* uniform on the fibers along $\boldsymbol{\nu}$, as Φ depends on x_3 .

Moreover, by (26), the three-dimensional right Cauchy-Green tensor \mathbf{C}_f can be written as

$$\mathbf{C}_f = \mathbf{C}_\Phi + \Phi'^2 \mathbf{e}_3 \otimes \mathbf{e}_3, \quad (29)$$

where

$$\mathbf{C}_\Phi := \mathbf{C} + \Phi \mathbf{C}_1 + \Phi^2 \mathbf{C}_2. \quad (30)$$

In (30),

$$\mathbf{C} := (\nabla \mathbf{y})^\top (\nabla \mathbf{y}) \quad (31)$$

is the two-dimensional right Cauchy-Green tensor,

$$\mathbf{C}_1 := 2(\nabla \mathbf{y})^\top (\nabla_s \boldsymbol{\nu})(\nabla \mathbf{y}), \quad \text{and} \quad \mathbf{C}_2 := (\nabla \mathbf{y})^\top (\nabla_s \boldsymbol{\nu})^2 (\nabla \mathbf{y}). \quad (32)$$

By (24), (29) becomes a (rather involved) function of the mapping \mathbf{y} and the variable x_3 .

Our next task is to integrate in the latter variable the expression for f_t in (20). To this end, we make further use of the *photo-uniformity* approximation discussed at the end of Sect. 2: we shall take $(\ell_\perp, \ell_\parallel)$ and S as *independent* of x_3 . In particular, by (28) and (23), in (9) we shall express \mathbf{n} as

$$\mathbf{n}(\mathbf{f}(\mathbf{x}, 0)) = \frac{(\nabla \mathbf{y}) \mathbf{n}_0}{|(\nabla \mathbf{y}) \mathbf{n}_0|} = \frac{(\nabla \mathbf{y}) \mathbf{n}_0}{(\mathbf{n}_0 \cdot \mathbf{C} \mathbf{n}_0)^{1/2}}, \quad (33)$$

which is the nematic director evaluated on \mathcal{S} and appears to be conveyed by the deformation of \mathcal{S}_0 , in accordance with the three-dimensional constraint (14). Accordingly, to mimic (15), we shall also assume that

$$\det \mathbf{C} = 1, \quad (34)$$

a constraint that predicates the *inextensibility* of the midsurface \mathcal{S}_0 .

Reasoning as in [19], we identify the stretching and bending *contents* of the surface *elastic* free energy, as the \mathbf{y} -dependent components scaling like h and h^3 , respectively, of the three-dimensional density f_t integrated in x_3 over the thickness of S . Denoting by F_s and F_b the resulting stretching and bending elastic contents, respectively, both *scaled* to $n_n k_B T h$, with essentially the same computations illustrated in [19], which would be too boring to reproduce here, we arrive at

$$\begin{aligned} F_s[S, \mathbf{y}; I] := \mu \int_{\mathcal{S}_0} \left\{ \frac{\ell_{0\perp}}{\ell_\perp} + \frac{\ell_{0\perp}}{\ell_\parallel} \operatorname{tr} \mathbf{C} + \frac{1}{\ell_\parallel} (\ell_{0\parallel} - \ell_{0\perp}) \mathbf{n}_0 \cdot \mathbf{C} \mathbf{n}_0 \right. \\ \left. - \ell_{0\perp} \left(\frac{1}{\ell_\parallel} - \frac{1}{\ell_\perp} \right) \frac{1}{\mathbf{n}_0 \cdot \mathbf{C} \mathbf{n}_0} \right\} dA \end{aligned} \quad (35)$$

and

$$\begin{aligned} F_b[S, \mathbf{y}; I] := \frac{1}{3} h^2 \mu \int_{\mathcal{S}_0} \left\{ 2 \frac{\ell_{0\perp}}{\ell_\perp} (8H^2 - K) \right. \\ - \left[\frac{\ell_{0\perp}}{\ell_\parallel} \operatorname{tr} \mathbf{C} + \frac{1}{\ell_\parallel} (\ell_{0\parallel} - \ell_{0\perp}) \mathbf{n}_0 \cdot \mathbf{C} \mathbf{n}_0 \right. \\ + 3 \ell_{0\perp} \left(\frac{1}{\ell_\parallel} - \frac{1}{\ell_\perp} \right) \frac{1}{\mathbf{n}_0 \cdot \mathbf{C} \mathbf{n}_0} \Big] K \\ \left. + 4 \ell_{0\perp} \left(\frac{1}{\ell_\parallel} - \frac{1}{\ell_\perp} \right) (2H - \kappa_n) \kappa_n \frac{1}{\mathbf{n}_0 \cdot \mathbf{C} \mathbf{n}_0} \right\} dA, \end{aligned} \quad (36)$$

where A here denotes the area measure and

$$\kappa_n := \mathbf{n} \cdot (\nabla_s \nu) \mathbf{n}. \quad (37)$$

F_s and F_b embody two separate components of the elastic free energy at the level of approximation we consider. To obtain the total free energy F_t (likewise scaled to $n_n k_B T h$), we must supplement $F_s + F_b$ with the integral (again across the slab's thickness) of the components of f_t independent of the deformation \mathbf{y} ,

$$F_t[S, \mathbf{y}; I] := F_s[S, \mathbf{y}; I] + F_b[S, \mathbf{y}; I] + \int_{\mathcal{S}_0} \left\{ \mu \left[\ln \frac{\ell_{\parallel}}{\ell_{0\parallel}} + 2 \ln \frac{\ell_{\perp}}{\ell_{0\perp}} \right] + 2(1 - \phi) \psi_{\text{MS}}(S) \right\} dA. \quad (38)$$

It is worth noting that by the scaling chosen here F_t has the physical dimensions of an area; to obtain a dimensionless energy, we should normalize F_t to the area of \mathcal{S}_0 (which by (34) is the same as the area of \mathcal{S}), as will be done in the following section.

If light is impinging at right angles from above on \mathcal{S}_0 , so that $\mathbf{k} = -\mathbf{e}_3$ (see Fig. 2), by (33), the *cis*-population fraction ϕ in (9) depends on \mathbf{k} and \mathbf{n} through

$$(\mathbf{n} \cdot \mathbf{k})^2 = \frac{(\mathbf{e}_3 \cdot (\nabla \mathbf{y}) \mathbf{n}_0)^2}{\mathbf{n}_0 \cdot \mathbf{C} \mathbf{n}_0}. \quad (39)$$

In [6], a few realistic values were suggested for the parameters that still need to be prescribed to solve a specific equilibrium problem. They suggested to take

$$A = \frac{1}{6}, \quad \frac{b}{a} = \frac{1}{2}, \quad \text{and} \quad S_0 \doteq 0.61, \quad \text{corresponding to } T \doteq 0.91 T_{\text{NI}}, \quad (40)$$

where T_{NI} is the nematic-to-isotropic transition temperature. In our parameterization of the Maier-Saupe potential ψ_{MS} in (18), this value of S_0 corresponds to $J \doteq 7.5$. As for the relative intensity I , Eisenbach [58] suggests that it should not exceed 15, whereas for Serra and Terentjev [59] it could go up to 80. In the application of our theory presented in following section, we shall take the above values for A , b/a , S_0 , and J , and we shall never consider going beyond $I = 70$.

4 Ribbon Deflection

We now consider a thin, narrow ribbon originally parallel to the $(\mathbf{e}_1, \mathbf{e}_2)$ plane. Its midsurface \mathcal{S}_0 is a narrow strip of length l and width w , represented by the set $\mathcal{S}_0 = \{(x_1, x_2) : 0 \leq x_1 \leq l, 0 \leq x_2 \leq w\}$. We further assume that the ribbon remains at all times homogeneous in x_2 and parallel to the \mathbf{e}_2 direction so that the scalar order parameter S is a function $S = S(x_1)$ of the x_1 coordinate only.

We represent \mathbf{y} as

$$\mathbf{y}(x_1, x_2) = y_1(x_1) \mathbf{e}_1 + y_2(x_2) \mathbf{e}_2 + y_3(x_1) \mathbf{e}_3, \quad (41)$$

which allows the ribbon to come out of the $(\mathbf{e}_1, \mathbf{e}_2)$ plane while its normal remains in the $(\mathbf{e}_1, \mathbf{e}_3)$ plane at all times.

In order to make the inextensibility constraint (34) explicit, we note that

$$\nabla \mathbf{y} = y'_1(x_1)\mathbf{e}_1 \otimes \mathbf{e}_1 + y'_2(x_2)\mathbf{e}_2 \otimes \mathbf{e}_2 + y'_3(x_1)\mathbf{e}_3 \otimes \mathbf{e}_1 \quad (42)$$

and so

$$\mathbf{C} = \{[y'_1(x_1)]^2 + [y'_3(x_1)]^2\} \mathbf{e}_1 \otimes \mathbf{e}_1 + [y'_2(x_2)]^2 \mathbf{e}_2 \otimes \mathbf{e}_2. \quad (43)$$

Hence, the requirement $\det \mathbf{C} = 1$ becomes

$$\{[y'_1(x_1)]^2 + [y'_3(x_1)]^2\} [y'_2(x_2)]^2 = 1. \quad (44)$$

Separation of variables shows that this is satisfied only if there are a scalar $\lambda > 0$ and a function ϑ such that

$$\mathbf{C} = \frac{1}{\lambda^2} \mathbf{e}_1 \otimes \mathbf{e}_1 + \lambda^2 \mathbf{e}_2 \otimes \mathbf{e}_2 \quad (45)$$

and

$$y_1(x_1) = \frac{1}{\lambda} \int_0^{x_1} \cos \vartheta(x) dx, \quad y_3(x_1) = \frac{1}{\lambda} \int_0^{x_1} \sin \vartheta(x) dx, \quad y_2(x_2) = \lambda x_2. \quad (46)$$

A value of $\lambda > 1$ corresponds to a contraction of the length of the ribbon together with an extension of its width.

The cross-section of the ribbon in the $(\mathbf{e}_1, \mathbf{e}_3)$ plane is described by the curve γ where

$$\gamma(x_1) = (y_1(x_1), y_3(x_1)). \quad (47)$$

As

$$\gamma'(x_1) = \left(\frac{1}{\lambda} \cos \vartheta(x_1), \frac{1}{\lambda} \sin \vartheta(x_1) \right), \quad (48)$$

we see that $\vartheta(x_1)$ is simply the angle that the tangent to the ribbon makes at $\mathbf{y}(x_1, x_2)$ with the \mathbf{e}_1 axis. A standard computation shows that there the curvature κ of the ribbon is

$$\kappa(x_1) = \lambda |\vartheta'(x_1)|. \quad (49)$$

4.1 Ribbon free energy

To make the free energy of the ribbon explicit, we write the director imprinted in \mathcal{S}_0 as

$$\mathbf{n}_0 = \cos \varphi_0 \mathbf{e}_1 + \sin \varphi_0 \mathbf{e}_2. \quad (50)$$

As before, we assume that unpolarized light is shone upon the ribbon from above with $\mathbf{k} = -\mathbf{e}_3$. The right-hand-side of equation (39) can now be

computed by using also (42), (45), and (46); we find that

$$(\mathbf{n} \cdot \mathbf{k})^2 = \frac{\sin^2 \vartheta \cos^2 \varphi_0}{\cos^2 \varphi_0 + \lambda^4 \sin^2 \varphi_0}. \quad (51)$$

At this point, it is worth remarking that the representation in (41) for \mathbf{y} and hence the expression (51) are realistic only for either $\varphi_0 = 0$ or $\varphi_0 = \frac{\pi}{2}$. For $0 < \varphi_0 < \frac{\pi}{2}$, a more general class of deformations \mathbf{y} should be considered, which also allows for twist. As can be seen from (51), the case $\varphi_0 = \frac{\pi}{2}$ is almost trivial, as the number fraction ϕ of *cis* molecules given by equation (9) would then be independent of ϑ . Therefore, we focus on the case $\varphi_0 = 0$, which will turn out to be rich enough to allow the ribbon to change shape.

The free energy density of the narrow ribbon is independent of x_2 , and so the total free energy F_t given by (38) can be simplified to

$$\begin{aligned} F_t[S, \lambda, \vartheta; I] := \int_0^l \left\{ \mu \left[\frac{4}{3} \lambda^2 h^2 \vartheta'^2 + \frac{\ell_{0\perp}}{\ell_{\perp}} + \frac{\ell_{0\perp}}{\ell_{\parallel}} \left(\frac{1}{\lambda^2} + \lambda^2 \right) \right. \right. \\ \left. \left. + \frac{1}{\ell_{\parallel}} (\ell_{0\parallel} - \ell_{0\perp}) \left(\frac{1}{\lambda^2} \cos^2 \varphi_0 + \lambda^2 \sin^2 \varphi_0 \right) \right. \right. \\ \left. \left. - \ell_{0\perp} \left(\frac{1}{\ell_{\parallel}} - \frac{1}{\ell_{\perp}} \right) \frac{\lambda^2}{\cos^2 \varphi_0 + \lambda^4 \sin^2 \varphi_0} \right. \right. \\ \left. \left. + \ln \frac{\ell_{\parallel}}{\ell_{0\parallel}} + 2 \ln \frac{\ell_{\perp}}{\ell_{0\perp}} \right] + 2(1 - \phi) \psi_{\text{MS}}(S) \right\} dx_1, \end{aligned} \quad (52)$$

where we have scaled to $n_n k_B T h w$ and only the integration over x_1 along the length of the ribbon remains.

Before introducing further simplifications, we give the free energy a dimensionless form by defining $\xi := x_1/l$; the energy further scaled to the length l of the ribbon then becomes

$$F_t[S, \lambda, \vartheta; I] = \int_0^1 \left\{ \frac{4}{3} \mu \left(\frac{h}{l} \right)^2 \lambda^2 \vartheta'^2 + f(\vartheta, \lambda, S; I) \right\} d\xi, \quad (53)$$

where

$$\begin{aligned} f(\vartheta, \lambda, S; I) := \mu \left[\frac{\ell_{0\perp}}{\ell_{\perp}} + \frac{\ell_{0\perp}}{\ell_{\parallel}} \left(\frac{1}{\lambda^2} + \lambda^2 \right) + \frac{1}{\ell_{\parallel}} (\ell_{0\parallel} - \ell_{0\perp}) \left(\frac{1}{\lambda^2} \cos^2 \varphi_0 + \lambda^2 \sin^2 \varphi_0 \right) \right. \\ \left. - \ell_{0\perp} \left(\frac{1}{\ell_{\parallel}} - \frac{1}{\ell_{\perp}} \right) \frac{\lambda^2}{\cos^2 \varphi_0 + \lambda^4 \sin^2 \varphi_0} + \ln \frac{\ell_{\parallel}}{\ell_{0\parallel}} + 2 \ln \frac{\ell_{\perp}}{\ell_{0\perp}} \right] \\ + 2(1 - \phi) \psi_{\text{MS}}(S). \end{aligned} \quad (54)$$

4.2 Clamped ribbon geometry

We consider a ribbon *clamped* at one end and *free* at the other. Specifically, we prescribe the boundary conditions

$$\vartheta(0) = 0 \quad \text{and} \quad \vartheta'(1) = 0, \quad (55)$$

that is, the curvature (49) vanishes at the free end. We assume that the director is imprinted so as to lie along the length of the ribbon, $\varphi_0 = 0$.

By symmetry, $\vartheta \equiv 0$ is always a critical point of F_t . Indeed, f in equation (54) is an *even* function of ϑ for all values of the intensity I , see (51). Therefore, all other critical points of F_t come in *pairs* of opposite signs, one member corresponding to an increasing function $y_3(\xi)$, the other to a decreasing function. We take the *increasing* companion as representative of each pair: $0 \leq \vartheta \leq \vartheta_m$, see the discussion at the end of Sect. 2. Figure 3 shows a sketch of two ribbons, one undistorted and the other in a bent configuration.

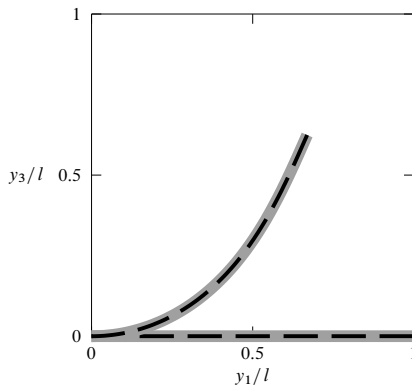


Fig. 3: The ribbon, depicted in grey, is clamped at the origin with its left end. Without illumination, it lies on the y_1 -axis. Upon illumination, its right end is free to rise, with the curvature at the free end prescribed to be zero. The black bars indicate the nematic director, which is aligned along the length of the ribbon.

The integrand in the free energy (53) has two distinct contributions: the first term depends only on the derivative ϑ' , and the second term, f as given by (54), depends only on ϑ . If we assume that ϑ is constant, then the entire integrand is constant. For given light intensity I , the free energy is then minimized if f is the minimum with respect to λ and S . In Fig. 4 we show the minimising values λ_0 and S_0 for the case $\vartheta \equiv 0$ and the two values $\mu = 1/10$ and $\mu = 1/50$ for $0 \leq I \leq 50$.

The magnitude of the deviation of S and λ from their values at zero light intensity remains very small for all intensities. Motivated by this observation,

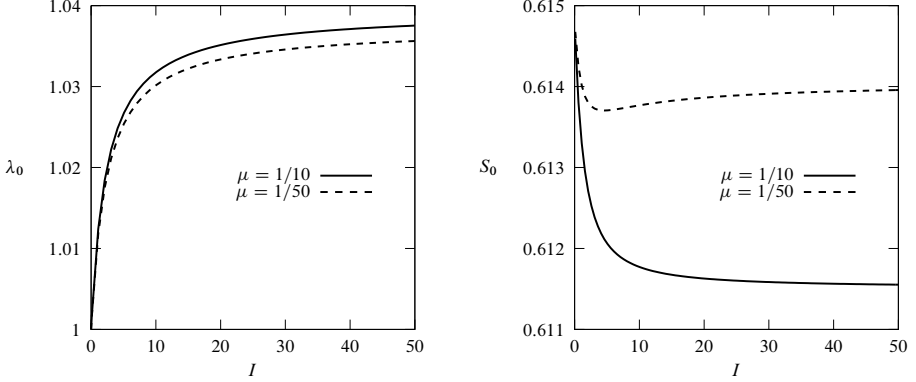


Fig. 4: Minimizers $(\lambda_0(I), S_0(I))$ of f in (54) for the given light intensity I and $\vartheta = 0$. These values also minimize the free energy (53) in the case $\vartheta \equiv 0$. Both the scalar order parameter S and the stretching λ vary on very slightly with the light intensity I . The situation is similar for other values of ϑ (not shown).

we make the following simplification. We replace f in (54) by

$$f_0(\vartheta; I) := f(\vartheta, \lambda_0(I), S_0(I); I) \quad (56)$$

where $\lambda_0(I)$ and $S_0(I)$ are the minimizers for f when $\vartheta = 0$. The energy functional then becomes

$$F_t[\vartheta; I] := \int_0^1 \left\{ \frac{4}{3} \mu \left(\frac{h}{l} \right)^2 [\lambda_0(I)]^2 \vartheta'^2 + f_0(\vartheta; I) \right\} d\xi, \quad (57)$$

which now depends on the single unknown function ϑ .

4.3 Euler-Lagrange equation

Any equilibrium profile of the ribbon needs to satisfy the Euler-Lagrange equation derived from (57),

$$\frac{8}{3} \mu [\lambda_0(I)]^2 \left(\frac{h}{l} \right)^2 \vartheta'' - \frac{\partial f_0(\vartheta; I)}{\partial \vartheta} = 0. \quad (58)$$

Since $\left. \frac{\partial f_0(\vartheta; I)}{\partial \vartheta} \right|_{\vartheta=0} = 0$, the profile of the undistorted ribbon with $\vartheta \equiv 0$ is always a solution of equation (58) satisfying the boundary conditions (55); we shall call it the *trivial* solution. We analyze equation (58) using a hybrid approach: We first derive a range of explicit expressions that then serve as a basis for producing numerically a range of illustrating graphs using the parameters given in (40).

For non-trivial solutions, multiplying equation (58) by ϑ' and integrating shows that a conservation law holds in the form

$$\frac{4}{3}\mu[\lambda_0(I)]^2\left(\frac{h}{l}\right)^2(\vartheta')^2 - f_0(\vartheta; I) = c \quad (59)$$

with a constant c . This constant can be determined by using the boundary condition $\vartheta'(1) = 0$, we have

$$c = -f_0(\vartheta(1); I). \quad (60)$$

Equation (59) is autonomous (i.e., it does not depend explicitly on ξ) and we are interested in its solutions with $\vartheta' \geq 0$. On every such solution, if existing, ϑ ranges monotonically in the interval $[0, \vartheta(1)]$, and so we find that $\vartheta(1) = \vartheta_m$, namely that the largest ribbon angle is found at the free end. Moreover, it readily follows from (48) that the corresponding equilibrium profile of the ribbon is *convex* (as sketched in Fig. 3).

Using the constant (60) in equation (59) we find that

$$\vartheta'(\xi) = \frac{d\vartheta}{d\xi} = \frac{l}{2h\lambda_0(I)}\sqrt{\frac{3}{\mu}}\sqrt{f_0(\vartheta(\xi); I) - f_0(\vartheta_m; I)}, \quad (61)$$

where for clarity we have here included the argument ξ . Separating variables and integrating yields

$$\xi = \frac{2h\lambda_0(I)}{l}\sqrt{\frac{\mu}{3}}\int_0^\vartheta \frac{d\eta}{\sqrt{f_0(\eta; I) - f_0(\vartheta_m; I)}}. \quad (62)$$

Recalling that $\vartheta(1) = \vartheta_m$, we find that

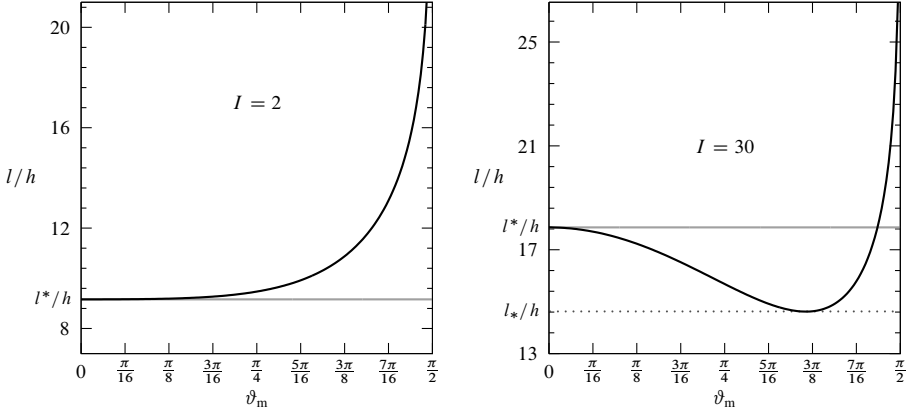
$$\frac{l}{h} = 2\lambda_0(I)\sqrt{\frac{\mu}{3}}\int_0^{\vartheta_m} \frac{d\vartheta}{\sqrt{f_0(\vartheta; I) - f_0(\vartheta_m; I)}}, \quad (63)$$

which is a compatibility condition for the solution profile. It links the ratio l/h of length to thickness of the ribbon, the light intensity I , and the maximum angle ϑ_m .

A condition for a bent solution to bifurcate from the trivial one can be obtained by computing the limit of equation (63) as $\vartheta_m \rightarrow 0$, assuming that it exists. To find the limit of the integral, we consider the Taylor series of f_0 near zero,

$$f_0(\vartheta) = f_0(0) + \frac{1}{2}f_0''(0)\vartheta^2 + O(\vartheta^4), \quad (64)$$

where, for brevity, the parameter I has been dropped from the argument of f_0 and a prime denotes differentiation with respect to ϑ . Use of (64) in (63)



(a) If l/h is less than l^*/h , there is no value for ϑ_m that allows for a bent profile, so the only possible equilibrium configuration is the trivial one. If l/h is greater than l^*/h , there is a single solution with a bent profile.

(b) For l/h less than the minimum l_*/h of the black graph, only the trivial solution exists. For l/h bigger than the minimum but less than l^*/h , two bent solutions exist. Finally, when $l/h > l^*/h$ there is only one bent solution.

Fig. 5: For $I = 2$ in (a) and $I = 30$ in (b) the black graph shows the values of l/h required to satisfy the compatibility condition (63) as a function of ϑ_m . The grey line shows the limit l^*/h of l/h as $\vartheta_m \rightarrow 0$, see equation (66). For $I = 2$, there are two different regimes depending on the value of l/h , while for $I = 30$, there are three regimes.

shows that the existence of the limit requires to have $f_0''(0) < 0$, as

$$\lim_{\vartheta_m \rightarrow 0} \int_0^{\vartheta_m} \frac{d\vartheta}{\sqrt{f_0(\vartheta) - f_0(\vartheta_m)}} = \sqrt{\frac{-2}{f_0''(0)}} \lim_{\vartheta_m \rightarrow 0} \int_0^{\vartheta_m} \frac{d\vartheta}{\sqrt{\vartheta_m^2 - \vartheta^2}} = \frac{\pi}{2} \sqrt{\frac{-2}{f_0''(0)}}, \quad (65)$$

and so a bifurcation is found when

$$\frac{l^*}{h} = \pi \lambda_0(I) \sqrt{\frac{-2\mu}{3f_0''(0)}}. \quad (66)$$

Figure 5 shows for the two intensities $I = 2$ and $I = 30$ the value of l^*/h as a grey horizontal line and, as a black graph, the values of l/h obtained using the compatibility condition (63) for $0 < \vartheta_m < \pi/2$. The two pictures are qualitatively very different. For the lower intensity, there is a single critical value l^*/h below which no bent solution is possible, and above which a single bent solution is present. For the higher intensity, in addition to l^*/h , there is a second critical value l_*/h below which no bent solution exist. For $l_*/h < l/h < l^*/h$ there are two bent solutions, and for $l/h > l^*/h$ there is a single bent solution, as in the other case.

To determine the critical value I_c of the intensity at which the two different behaviours meet, we examine the compatibility condition (63) for small values of ϑ_m . To this end, we need one further term of the Taylor series of f_0 near zero,

$$f_0(\vartheta) = f_0(0) + \frac{1}{2}f_0''(0)\vartheta^2 + \frac{1}{24}f_0^{(iv)}(0)\vartheta^4 + O(\vartheta^6). \quad (67)$$

A straightforward computation then shows that

$$\int_0^{\vartheta_m} \frac{d\vartheta}{\sqrt{f_0(\vartheta) - f_0(\vartheta_m)}} = \frac{\pi}{2} \sqrt{\frac{-2}{f_0''(0)}} \left(1 - \frac{1}{16} \vartheta_m^2 \frac{f_0^{(iv)}(0)}{f_0''(0)} \right) + O(\vartheta_m^4). \quad (68)$$

Therefore, given that $-f_0''(0)$ is positive, when $f_0^{(iv)}(0)$ is positive we have the situation shown in Fig. 5 (a) with a single critical value l^*/h . When $f_0^{(iv)}(0)$ is negative we have the situation shown in Fig. 5 (b) with the additional critical value l_*/h .

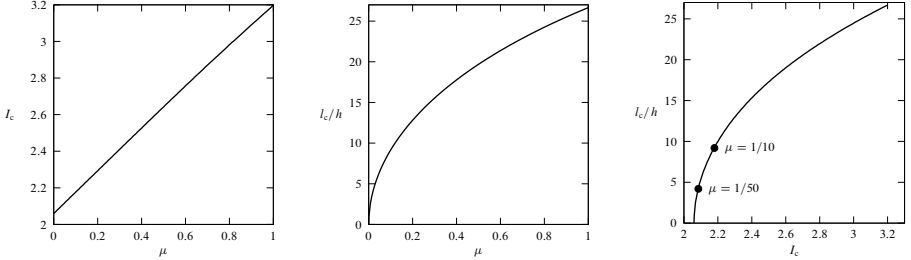


Fig. 6: Critical intensity I_c (left) and critical length l_c/h (middle) versus μ and the curve $(I_c, l_c/h)$ parameterized by μ (right) with the relevant values of μ marked by black circles. For length-to-thickness ratios below the graph in the middle diagram, no bent solutions exist for any intensity.

On the left of Fig. 6 we show for the whole possible range $0 \leq \mu \leq 1$ the critical values I_c of the intensity where the fourth derivative of f_0 at zero changes sign and in the middle the corresponding critical values l_c/h obtained by equation (66), $l_c = l^*(\mu, I_c)$. On the right, parametrized by μ , we plot the curve of critical points $(I_c, l_c/h)$ in the I - l/h plane.

To assess the stability of bent ribbon profiles relative to the $\vartheta \equiv 0$ profile, we compare energies. In this (limited) perspective we shall say that an equilibrium configuration is stable if it has less energy than any other configuration.

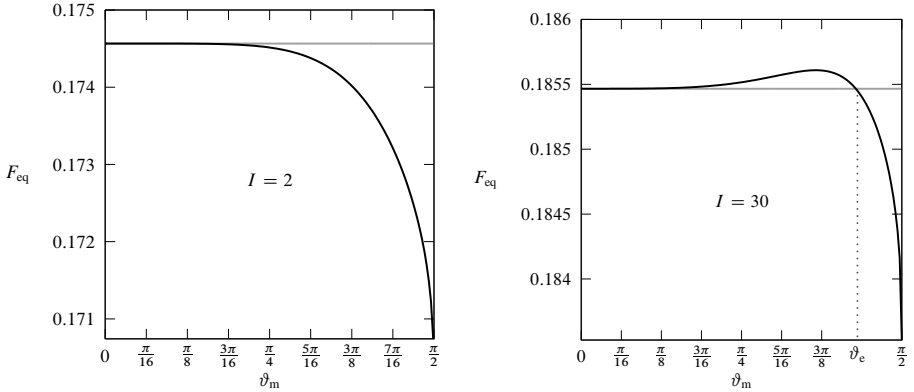
The total energy of the ribbon in an equilibrium configuration can be expressed as a function of ϑ_m by using in the functional (57) the conservation law (59) with the constant from (60):

$$F_{\text{eq}}(\vartheta_m; I) = \int_0^1 \{f_0(\vartheta; I) - f_0(\vartheta_m; I) + f_0(\vartheta; I)\} d\xi$$

$$\begin{aligned}
&= \int_0^{\vartheta_m} \left\{ \frac{2f_0(\vartheta; I) - f_0(\vartheta_m; I)}{\sqrt{f_0(\vartheta; I) - f_0(\vartheta_m; I)}} \frac{2h\lambda_0(I)}{l} \sqrt{\frac{\mu}{3}} \right\} d\vartheta \\
&= \frac{1}{\int_0^{\vartheta_m} \frac{d\vartheta}{\sqrt{f_0(\vartheta; I) - f_0(\vartheta_m; I)}}} \int_0^{\vartheta_m} \frac{2f_0(\vartheta; I) - f_0(\vartheta_m; I)}{\sqrt{f_0(\vartheta; I) - f_0(\vartheta_m; I)}} d\vartheta, \quad (69)
\end{aligned}$$

where in the first step we have used equation (61) for substituting ξ with ϑ , and in the second step we have used the condition (63) to replace l/h .

Figure 7 shows the energy of equilibrium solutions for the same two intensities used in Fig. 5, $I = 2$ and $I = 30$, for $0 \leq \vartheta_m \leq \frac{\pi}{2}$. The value of l/h is implicitly defined by the compatibility condition (63). For $I < I_c$ (Fig. 7 (a)), if a bent solution exists it is always stable. For $I > I_c$ (Fig. 7 (b)), there can be both unstable and stable bent solutions; the maximum of F_{eq} is attained for the same value of ϑ_m as the minimum l_*/h of the function defined by (63) (see Fig. 5 (b)). As l/h is increased above l_*/h two bent solutions originate whose energies fall on either side of the maximum in Fig. 7 (b). As l/h keeps increasing, the solution with the smaller ϑ_m gradually approaches the trivial solution, having always higher energy until it merges with it at $l/h = l^*/h$. Correspondingly, the solution with larger ϑ_m keeps reducing its energy: there



(a) For $I = 2$, if a bent solutions exists, it is always stable as it has lower energy than the trivial solution.

(b) For $I = 30$, both bent solutions with lower and with higher energy than the trivial solution exist, compare Fig. 5 (b). There is exactly one bent solution with the same energy as the trivial solution; its corresponding angle ϑ_m is marked in the figure as ϑ_e .

Fig. 7: Energy of equilibrium solutions for $I = 2$ and $I = 30$ as a function of $0 \leq \vartheta_m \leq \frac{\pi}{2}$. The length l/h of the ribbon is implicitly determined by the compatibility condition (63) and can be read off from Fig. 5. For reference, the grey line shows the energy of the undistorted ribbon.

is then exactly one bent solution with the same energy as the trivial solution; we denote its maximum deflection angle ϑ_m by ϑ_e and the corresponding length to thickness ratio by l_e/h .

4.4 Bifurcation analysis

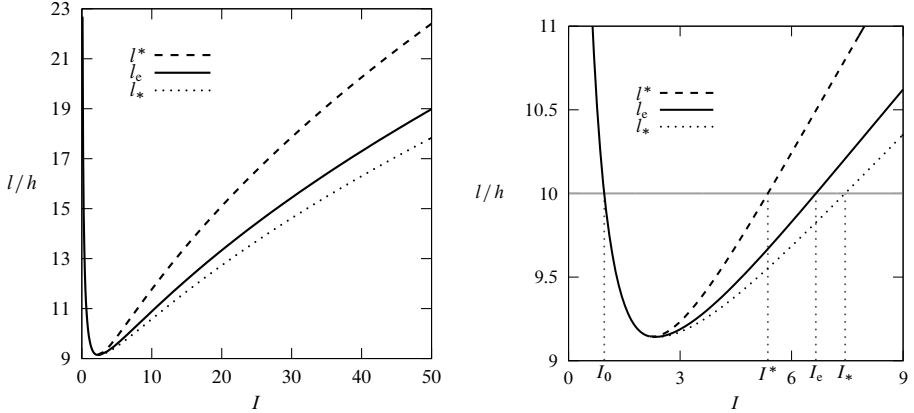


Fig. 8: Critical lengths versus light intensity for $\mu = 1/10$. Along the solid line, a bent solution exists that has the same energy as the trivial solution. Above the dashed line, the trivial solution is unstable. Below the dotted line, no bent solution exists. To the left of the minimum, located at the critical point $(I_c, l_c/l)$, all three critical lengths coincide and only the solid line is drawn: below it no bent solution exists, above it the trivial solution is unstable. In the blow-up on the right the grey line marks $l/h = 10$, and its intersections with the graphs are marked I_0 , I^* , I_e , and I_* : the same intensities are also identified in Fig. 9 below.

To summarize what we have established so far, we present in Fig. 8 three graphs in the I - l/h plane: the solid line shows l_e/h , where a bent solution exists that has the same energy as the trivial solution. The dashed line shows l^*/h as given by (66): above this line the trivial solution is unstable. The dotted line corresponds to the minimum l_*/h of the graph shown in Fig. 5 (b): below this line, no bent solution exists. The minimum of the graph in Fig. 8 has coordinates $(I_c, l_c/h)$ for the chosen value of $\mu = 1/10$, see the right graph in Fig. 6.

While Fig. 8 contains the gist of our analysis, it is rather artificial in that it shows length-to-thickness ratios as functions of the light intensity. Of course, in an experiment l/h is fixed and only I can be varied. We display therefore in Fig. 9 the maximum angle ϑ_m of the ribbon profile as a function of the intensity. When the light intensity reaches I_0 , a bifurcation from the trivial to a bent solution occurs. With increasing intensity, the maximum angle ϑ_m first increases but eventually decreases, and at I_* the bent solution disappears

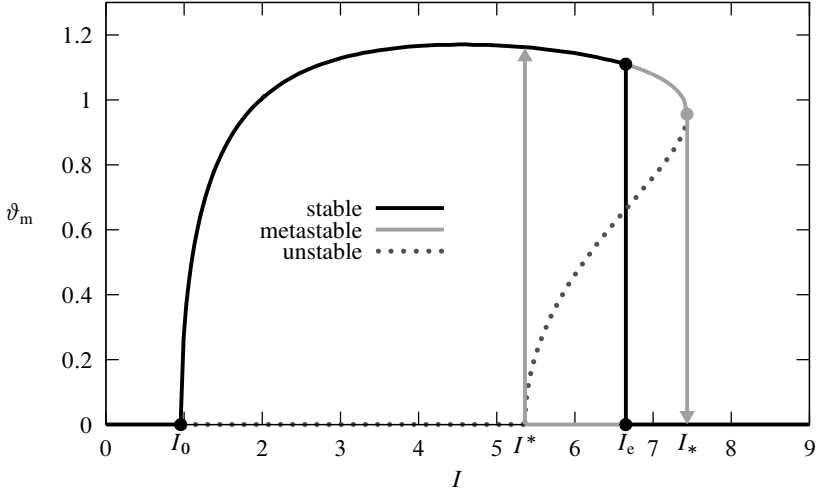


Fig. 9: Bifurcation diagram for $l/h = 10$. The intensities marked I_0 , I^* , I_e , and I_* correspond to those shown in the right graph in Fig. 8. As the intensity is increased from zero, at I_0 the trivial solution becomes unstable and a bent solution bifurcates up from $\vartheta = 0$. At I^* , the trivial solution enters the scene again, but here has higher energy than the bent solution. Both solutions have equal energy at I_e , and for intensities above I_* no bent solution exists any more.

altogether. Upon then decreasing the light intensity, the trivial solution can be continued up to I^* , where it merges with the unstable bent solution. In the interval between I^* and I_* there are *three* equilibria, the trivial solution and *two* bent solutions; our elementary stability taxonomy is not sufficient to cover all cases: we then call *metastable* the solution with intermediate energy, and *stable* (as before) the one with the least energy (see Fig. 9). One bent solution is stable in (I^*, I_e) and the trivial solution is metastable, whereas the trivial solution is stable in (I_e, I_*) and the same bent solution is metastable. In both intervals one bent solution is always unstable, the one that merges with the trivial solution at I^* . The intensities I^* and I_* delimit a *hysteresis* loop, which encloses the intensity I_e where the stable bent solution has the same energy as the trivial solution; there a first-order *shape transition* takes place, which could be seen as an abrupt *snapping* back and forth of the ribbon.

The picture is similar for all values of $l/h > l_c/h$. As an example, we show in Fig. 10 the bifurcation diagram for $l/h = 20$. For $l/h < l_c/h$, there is literally nothing to see: no bent solutions exist for any value of the intensity.

Finally, we show in Fig. 11 numerically computed solutions of the Euler-Lagrange equation (58) satisfying the boundary conditions (55). The parameters used are $\mu = 1/10$ and $l/h = 10$ for a range of intensities between $I = 1.25$ and $I = 8.25$, as shown. The angles of the ribbon on its right end coincide with the values of ϑ_m shown in Fig. 9.

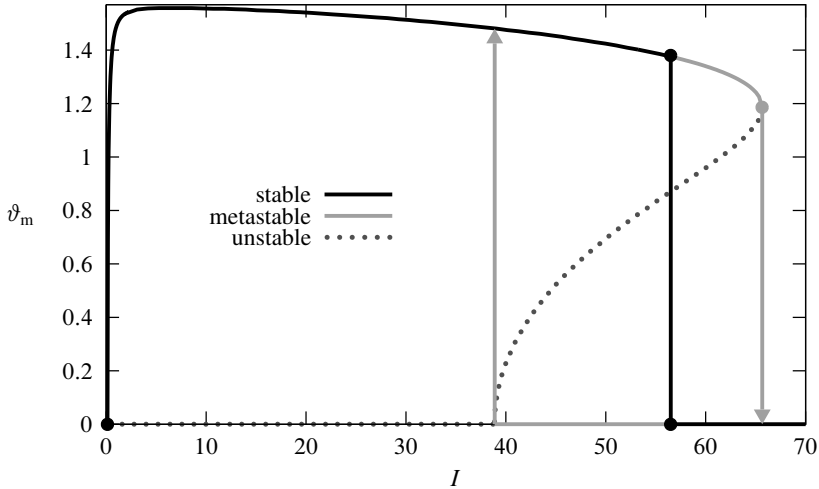


Fig. 10: Bifurcation diagram for $l/h = 20$. The structure is the same as in Fig. 9. The relatively longer ribbon here leads to a bent solution that both occurs at a lower intensity and is sustained for higher intensities. Also, the maximum angle is closer to $\pi/2$.

5 Conclusions

We presented a continuum model for photoresponsive elastomers, whose deformation is driven by illumination. The (dynamical) interaction of light with a nematogenic polymer network (hosting photoresponsive molecules) was described within the statistical mechanics model of Corbett and Warner [6, 7].

Light is responsible for a change in shape of photoresponsive molecules, which, once activated, deplete the nematic phase, and so have an effect on the nematic scalar order parameter S . This is what makes these materials different from ordinary nematic elastomers, where a change in S is thermally induced. The spontaneous deformation that ensues photoactivation is likely to change illumination conditions, and this in turn may either enhance or hamper deformation.

Our main objective was to study the equilibrium of a ribbon illuminated at right angles on one face in its undeformed configuration. To this end, we performed the reduction of the total free-energy functional to a thin planar sheet and applied our reduced theory to a ribbon with a realistic choice of physical parameters collected from the specialized literature. We found the equilibrium configurations of the illuminated ribbon with the nematic director frozen along its longer side and represented in closed form their bifurcation scenario.

We proved that the activation process is neither linear nor monotonic: the deflection of an activated ribbon first increases as expected, but then decreases before vanishing abruptly upon increasing the light intensity I above a critical value I_e , where the ribbon undergoes a first-order *shape transition*. A hysteresis

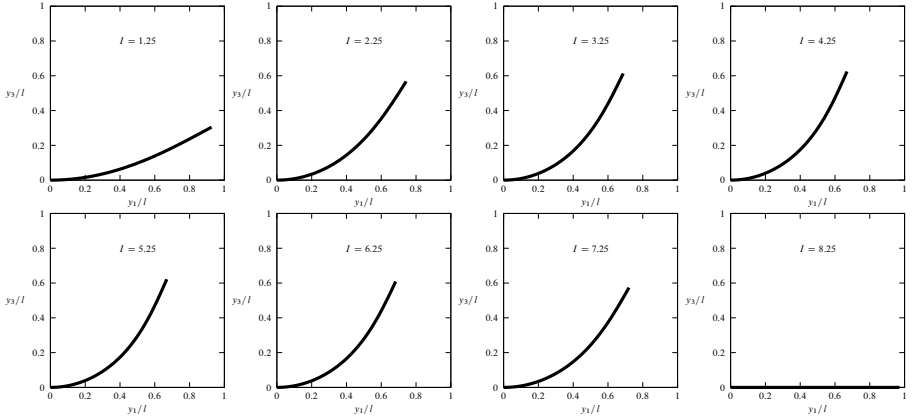


Fig. 11: Ribbon profiles for varying intensities with $\mu = 1/10$ and $l/h = 10$. Without illumination, the ribbon occupies the entire space on the y_1 axis between zero and one. When the illumination intensity exceeds a threshold value, the ribbon begins to extend upwards. With increasing intensity, the ribbon first extends further up before reaching a maximum height. For even higher extensivities, the height first decreases before the ribbon eventually snaps back to the y_1 axis. In the final picture shown, the ribbon is back on the y_1 axis but does not reach the point $y_1 = 1$ because for $I > 0$ also $\lambda > 1$.

cycle is present about $I = I_e$, featuring two metastable configurations of the ribbon. Our bifurcation analysis has also shown that for a given length of the ribbon there is an optimal value of I for which the deflection is maximum.

While deflections and displacements are generally large, dilations and contractions in an illuminated ribbon remain small. However, there is a critical length of the ribbon (depending only on the degree of cross-linking in the material) below which *no* deflection can be promoted by light, no matter how intense this is: the system is too stiff to gain energy by bending.

Heuristically, the non-monotonic response of an illuminated ribbon, with its abrupt fall, could be explained by the coupling between the *cis*-population fraction ϕ and the illumination angle that the direction of propagation of light \mathbf{k} makes with the nematic director \mathbf{n} (tangent to the ribbon's longer side in our case). We remarked that for $S > 0$ this coupling is most effective when \mathbf{k} and \mathbf{n} are orthogonal; when the spontaneous deformation reduces the illumination angle, photoactivation is reduced, resulting in a negative feedback.

In more mundane terms, we may say that when activating a ribbon with light, we should be *gentle*: too high an intensity may easily result in no deflection.

Our theory has limitations too. Perhaps the most conspicuous one is the *photo-uniformity* approximation that has been used at various stages. Since we do not account for partial penetration of light in the ribbon's cross-section, deflection either towards light or away from it would have precisely the same

energy cost. That deflection actually takes place *towards* light (as experimentally observed) should be inferred from *ad hoc* extrinsic considerations. Attempts have recently been made to account for the consequences that partial penetration of light has for the spontaneous deformation of thin flat bodies [8, 38].

Actually, a non-monotonic effect of light intensity upon deformation was also found in [8], but it was predicted to vanish gradually for very large intensities, not with the abrupt decay shown here. We have found in our simplified approach that very same lack of monotonicity, which can have important consequences in applications. This establishes that partial penetration of light is not solely responsible for it.

Appendix A About the Corbett-Warner Model

In this Appendix, which has a pedagogical character, we give details about the statistical model by Corbett and Warner presented in Sect. 2. Its contents are derived, with minor modifications and adaptations, from [6] and [18] (see also [52]).

A.1 Step tensors

A polymer strand in the reference configuration is represented as a chain of N rigid rods, each of length a , freely jointed one to the adjacent ones, so that the orientation $\mathbf{u}_i \in \mathbb{S}^2$ of the i th rod is completely independent from the orientation $\mathbf{u}_j \in \mathbb{S}^2$ of any other rod with $j \neq i$.¹²

The *span vector* vector \mathbf{R}_0 joining the ends of a strand is thus defined as

$$\mathbf{R}_0 := a \sum_{i=1}^N \mathbf{u}_i \quad (\text{A1})$$

and the *step tensor* \mathbf{L}_0 is correspondingly given by

$$\mathbf{L}_0 := \frac{3}{Na} \langle \mathbf{R}_0 \otimes \mathbf{R}_0 \rangle, \quad (\text{A2})$$

where the brackets $\langle \cdots \rangle$ denote ensemble averaging, as in the main text. By the mutual independence of rods, also in view of (1) written for \mathbf{Q}_0 and (A2), we readily arrive at

$$\mathbf{L}_0 = \frac{3Na^2}{Na} \langle \mathbf{u} \otimes \mathbf{u} \rangle = a(3\mathbf{Q}_0 + \mathbf{I}). \quad (\text{A3})$$

¹²It should perhaps be recalled that both photoresponsive molecules in the *trans* configuration and photoinert mesogens are treated on the same footing in the reference configuration.

Use of the uniaxial representation for \mathbf{Q}_0 in (A3) leads us straight to (4a) and (5). It is perhaps worth noting that for $\mathbf{Q}_0 = \mathbf{0}$, which represents the isotropic distribution, $\mathbf{L}_0 = a\mathbf{I}$, which accordingly represents a globule of radius a , thus justifying the scaling in definition (A2).

To give the principal chain steps $(\ell_\perp, \ell_\parallel)$ featuring in (4b) the expressions in (6) we must recall that in the present configuration rods of different lengths coexist in one and the same polymer strand, while obeying different statistics: photoinert rods of length a are in the nematic phase, whereas photoactivated rods of length $b < a$ are in the isotropic phase. Letting ϕ be the number fraction of the latter, there will be $(1 - \phi)N$ rods of length a and ϕN rods of length b , so that the span vector \mathbf{R} can be written as

$$\mathbf{R} = a \sum_{i=1}^{(1-\phi)N} \mathbf{u}_i + b \sum_{j=1}^{\phi N} \mathbf{v}_j, \quad (\text{A4})$$

where $\mathbf{u}_i \in \mathbb{S}^2$ and $\mathbf{v}_j \in \mathbb{S}^2$ are unit vectors along photoinert and photoactivated molecules, respectively. Now, \mathbf{u}_i and \mathbf{v}_j are clearly independent from one another, so that for \mathbf{u} and \mathbf{v} representative of their ensembles,

$$\langle \mathbf{u} \otimes \mathbf{v} \rangle = \mathbf{0}. \quad (\text{A5a})$$

Moreover, the \mathbf{v} 's are assumed to be distributed isotropically,

$$\langle \mathbf{v} \otimes \mathbf{v} \rangle = \frac{1}{3} \mathbf{I}, \quad (\text{A5b})$$

and the \mathbf{u} 's uniaxially,

$$\langle \mathbf{u} \otimes \mathbf{u} \rangle = \mathbf{Q} + \frac{1}{3} \mathbf{I}, \quad (\text{A5c})$$

with \mathbf{Q} as in (2). Making use of all equations (A5) to evaluate the average $\langle \mathbf{R} \otimes \mathbf{R} \rangle$ from (A4) and normalizing \mathbf{L} to the length Na of the unirradiated polymer, precisely as in (A2), we readily arrive at equations (4b) and (6) in the main text.

A.2 Equilibrium *cis*-population

We follow [5, 6], in the reinterpretation given in [18], to calculate the number fraction ϕ of photoresponsive molecules in the *cis*-state resulting from a dynamical equilibrium between forward and backward isomerizations.

Let N be, as above, the total number of monomers in a polymer strand and let A be the fraction of photoresponsive molecules among them. Thus, denoting by N_t the number of *trans*-molecules and by N_c the number of *cis*-molecules, conservation of mass requires that

$$N_t + N_c = AN. \quad (\text{A6})$$

The forward reaction rate $r_{t \rightarrow c}$ is proportional to the product of N_t and the average projected light intensity along the molecular direction \mathbf{u} ,

$$r_{t \rightarrow c} = \Gamma E^2 \langle (\mathbf{u} \cdot \mathbf{e})^2 \rangle_t N_t, \quad (\text{A7})$$

where Γ is a constant, $\mathbf{E} = E\mathbf{e}$ is the wave electric field, and the average $\langle \cdots \rangle_t$ should only be computed on the *trans*-molecules. However, since the latter obey the same statistics as all nematogenic molecules, the partial *trans*-average is just the same as the full average,

$$\langle (\mathbf{n} \cdot \mathbf{e})^2 \rangle_t = \langle (\mathbf{n} \cdot \mathbf{e})^2 \rangle. \quad (\text{A8})$$

The thermally induced backward reaction has a rate simply proportional to N_c ,

$$r_{c \rightarrow t} = \frac{1}{\tau} N_c, \quad (\text{A9})$$

where τ is a thermal relaxation time. Equilibrium requires that $r_{t \rightarrow c} = r_{c \rightarrow t}$. Inserting (A9), (A8), and (A7) into this equality, we easily see that

$$\phi = \frac{N_c}{N} = A \frac{I \langle (\mathbf{e} \cdot \mathbf{n})^2 \rangle}{1 + I \langle (\mathbf{e} \cdot \mathbf{n})^2 \rangle}, \quad (\text{A10})$$

where I is as in (10) with

$$\mathcal{I} = E^2 \quad \text{and} \quad \mathcal{I}_c = \frac{1}{\tau \Gamma}. \quad (\text{A11})$$

To obtain (7) from (A10), it now suffices to observe that

$$\langle (\mathbf{e} \cdot \mathbf{n})^2 \rangle = \mathbf{e} \cdot \langle \mathbf{u} \otimes \mathbf{u} \rangle \mathbf{e} = S(\mathbf{n} \cdot \mathbf{e})^2 + \frac{1}{3}(1 - S), \quad (\text{A12})$$

where use has also been made of (1) and (2).

References

- [1] Corbett, D., Modes, C.D., Warner, M.: Photomechanics: Bend, curl, topography, and topology. In: White, T.J. (ed.) *Photomechanical Materials, Composites, and Systems. Wireless Transduction of Light Into Work*, pp. 79–116. John Wiley & Sons, Hoboken, NJ (2017)
- [2] Finkelmann, H., Nishikawa, E., Pereira, G.G., Warner, M.: A new optomechanical effect in solids. *Phys. Rev. Lett.* **87**, 015501 (2001). <https://doi.org/10.1103/PhysRevLett.87.015501>
- [3] Eisenbach, C.D.: Isomerization of aromatic azo chromophores in poly(ethyl acrylate) networks and photomechanical effect. *Polymer*

- 21**(10), 1175–1179 (1980). [https://doi.org/10.1016/0032-3861\(80\)90083-X](https://doi.org/10.1016/0032-3861(80)90083-X)
- [4] Stolbova, O.V.: Calculation of the stationary value of a reversible photodichroism of viscous solutions. *Dokl. Akad. Nauk SSSR* **149**, 84–87 (1963). [*Sov. Phys. Dokl.* **8**, 275 (1963)]
- [5] Corbett, D., Warner, M.: Nonlinear photoresponse of disordered elastomers. *Phys. Rev. Lett.* **96**, 237802 (2006). <https://doi.org/10.1103/PhysRevLett.96.237802>
- [6] Corbett, D., Warner, M.: Polarization dependence of optically driven polydomain elastomer mechanics. *Phys. Rev. E* **78**, 061701 (2008). <https://doi.org/10.1103/PhysRevE.78.061701>
- [7] Corbett, D., Warner, M.: Linear and nonlinear photoinduced deformations of cantilevers. *Phys. Rev. Lett.* **99**, 174302 (2007). <https://doi.org/10.1103/PhysRevLett.99.174302>
- [8] Corbett, D., Xuan, C., Warner, M.: Deep optical penetration dynamics in photobending. *Phys. Rev. E* **92**, 013206 (2015). <https://doi.org/10.1103/PhysRevE.92.013206>
- [9] Bladon, P., Terentjev, E.M., Warner, M.: Deformation-induced orientational transitions in liquid crystals elastomer. *J. Phys. II France* **4**(1), 75–91 (1994). <https://doi.org/10.1051/jp2:1994100>
- [10] Warner, M., Gelling, K.P., Vilgis, T.A.: Theory of nematic networks. *J. Chem. Phys.* **88**(6), 4008–4013 (1988). <https://doi.org/10.1063/1.453852>
- [11] Warner, M., Wang, X.J.: Elasticity and phase behavior of nematic elastomers. *Macromolecules* **24**(17), 4932–4941 (1991). <https://doi.org/10.1021/ma00017a033>
- [12] Warner, M., Mostajeran, C.: Nematic director fields and topographies of solid shells of revolution. *Proc. R. Soc. London A* **474**(2210), 20170566 (2018). <https://doi.org/10.1098/rspa.2017.0566>
- [13] Warner, M., Terentjev, E.M.: *Liquid Crystal Elastomers*. International Series of Monographs on Physics, vol. 120. Oxford University Press, New York (2003)
- [14] White, T.J.: Photomechanical effects in liquid-crystalline polymer networks and elastomers. In: White, T.J. (ed.) *Photomechanical Materials, Composites, and Systems. Wireless Transduction of Light Into Work*, pp. 153–177. John Wiley & Sons, Hoboken, NJ (2017)

- [15] Modes, C.D., Bhattacharya, K., Warner, M.: Disclination-mediated thermo-optical response in nematic glass sheets. *Phys. Rev. E* **81**, 060701 (2010). <https://doi.org/10.1103/PhysRevE.81.060701>
- [16] Ware, T.H., White, T.J.: Programmed liquid crystal elastomers with tunable actuation strain. *Polym. Chem.* **6**, 4835–4844 (2015). <https://doi.org/10.1039/C5PY00640F>
- [17] Maier, W., Saupe, A.: Eine einfache molekulare Theorie des nematischen kristallinflüssigen Zustandes. *Z. Naturforsch.* **13a**, 564–566 (1958). Translated into English in [60], pp. 381–385.
- [18] Bai, R., Bhattacharya, K.: Photomechanical coupling in photoactive nematic elastomers. *J. Mech. Phys. Solids* **144**, 104115 (2020). <https://doi.org/10.1016/j.jmps.2020.104115>
- [19] Ozenda, O., Sonnet, A.M., Virga, E.G.: A blend of stretching and bending in nematic polymer networks. *Soft Matter* **16**, 8877–8892 (2020). <https://doi.org/10.1039/D0SM00642D>
- [20] Ozenda, O., Virga, E.G.: On the Kirchhoff-Love hypothesis (revised and vindicated). *J. Elast.* **143**, 359–384 (2021). <https://doi.org/10.1007/s10659-021-09819-7>
- [21] Warner, M., Bladon, P., Terentjev, E.M.: “Soft elasticity”—deformation without resistance in liquid crystal elastomers. *J. Phys. II France* **4**(1), 93–102 (1994). <https://doi.org/10.1051/jp2:1994116>
- [22] Terentjev, E.M., Warner, M., Bladon, P.: Orientation of nematic elastomers and gels by electric fields. *J. Phys. II France* **4**(4), 667–676 (1994). <https://doi.org/10.1051/jp2:1994154>
- [23] Verwey, G.C., Warner, M.: Soft rubber elasticity. *Macromolecules* **28**(12), 4303–4306 (1995). <https://doi.org/10.1021/ma00116a036>
- [24] Verwey, G.C., Warner, M.: Multistage crosslinking of nematic networks. *Macromolecules* **28**(12), 4299–4302 (1995). <https://doi.org/10.1021/MA00116A035>
- [25] Verwey, G.C., Warner, M., Terentjev, E.M.: Elastic instability and stripe domains in liquid crystalline elastomers. *J. Phys. II France* **6**(9), 1273–1290 (1996). <https://doi.org/10.1051/jp2:1996130>
- [26] Anderson, D.R., Carlson, D.E., Fried, E.: A continuum-mechanical theory for nematic elastomers. *J. Elast.* **56**, 33–58 (1999). <https://doi.org/10.1023/A:1007647913363>

- [27] Zhang, Y., Xuan, C., Jiang, Y., Huo, Y.: Continuum mechanical modeling of liquid crystal elastomers as dissipative ordered solids. *J. Mech. Phys. Solids* **126**, 285–303 (2019). <https://doi.org/10.1016/j.jmps.2019.02.018>
- [28] Mihai, L.A., Wang, H., Guilleminot, J., Goriely, A.: Nematic liquid crystalline elastomers are aeolotropic materials. *Proc. R. Soc. London A* **477**(2253), 20210259 (2021). <https://doi.org/10.1098/rspa.2021.0259>
- [29] White, T.J. (ed.): *Photomechanical Materials, Composites, and Systems: Wireless Transduction of Light Into Work*. John Wiley & Sons, Hoboken, New Jersey (2017)
- [30] Korley, L.T.J., Ware, T.H.: Introduction to special topic: Programmable liquid crystal elastomers. *J. Appl. Phys.* **130**(22), 220401 (2021). <https://doi.org/10.1063/5.0078455>
- [31] Mahimwalla, Z., Yager, K.G., Mamiya, J.-i., Shishido, A., Priimagi, A., Barrett, C.J.: Azobenzene photomechanics: prospects and potential applications. *Polym. Bull.* **69**, 967–1006 (2012). <https://doi.org/10.1007/s00289-012-0792-0>
- [32] Ube, T., Ikeda, T.: Photomobile polymer materials with crosslinked liquid-crystalline structures: Molecular design, fabrication, and functions. *Angew. Chem. Int. Ed.* **53**(39), 10290–10299 (2014). <https://doi.org/10.1002/anie.201400513>
- [33] White, T.J.: Photomechanical effects in liquid crystalline polymer networks and elastomers. *J. Polym. Sci. Part B: Polym. Phys.* **56**(9), 695–705 (2018). <https://doi.org/10.1002/polb.24576>
- [34] Ula, S.W., Traugutt, N.A., Volpe, R.H., Patel, R.R., Yu, K., Yakacki, C.M.: Liquid crystal elastomers: an introduction and review of emerging technologies. *Liquid Cryst. Rev.* **6**(1), 78–107 (2018). <https://doi.org/10.1080/21680396.2018.1530155>
- [35] Pang, X., Lv, J.-a., Zhu, C., Qin, L., Yu, Y.: Photodeformable azobenzene-containing real polymers and soft actuators. *Adv. Mater.* **31**(52), 1904224 (2019). <https://doi.org/10.1002/adma.201904224>
- [36] Kuenstler, A.S., Hayward, R.C.: Light-induced shape morphing of thin films. *Curr. Opin. Colloid & Interface Sci.* **40**, 70–86 (2019). <https://doi.org/10.1016/j.cocis.2019.01.009>
- [37] Warner, M.: Topographic mechanics and applications of liquid crystalline solids. *Annu. Rev. Condens. Matter Phys.* **11**(1), 125–145 (2020). <https://doi.org/10.1146/annurev-conmatphys-031119-050738>

- [38] Korner, K., Kuenstler, A.S., Hayward, R.C., Audoly, B., Bhattacharya, K.: A nonlinear beam model of photomotile structures. *Proc. Natl. Acad. Sci. USA* **117**(18), 9762–9770 (2020). <https://doi.org/10.1073/pnas.1915374117>
- [39] Goriely, A., Moulton, D.E., Mihai, L.A.: A rod theory for liquid crystalline elastomers. *J. Elast.* (2022). <https://doi.org/10.1007/s10659-021-09875-z>
- [40] Virga, E.G.: *Variational Theories for Liquid Crystals*. Applied Mathematics and Mathematical Computation, vol. 8. Chapman & Hall, London (1994)
- [41] Beer, A.: Bestimmung der Absorption des rothen Lichts in farbigen Flüssigkeiten. *Ann. Phys.* **162**(5), 78–88 (1852). <https://doi.org/10.1002/andp.18521620505>
- [42] Fox, M.: *Optical Properties of Solids*, 2nd edn. Oxford University Press, Oxford (2010)
- [43] Yu, Y., Nakano, M., Ikeda, T.: Directed bending of a polymer film by light. *Nature*. **425**, 145 (2003). <https://doi.org/10.1038/425145a>
- [44] Liu, L., del Pozo, M., Mohseninejad, F., Debije, M.G., Broer, D.J., Schenning, A.P.H.J.: Light tracking and light guiding fiber arrays by adjusting the location of photoresponsive azobenzene in liquid crystal networks. *Adv. Optical Mater.* **8**(18), 2000732 (2020). <https://doi.org/10.1002/adom.202000732>
- [45] Camacho-Lopez, M., Finkelmann, H., Palfy-Muhoray, P., Shelley, M.: Fast liquid-crystal elastomer swims into the dark. *Nature Mater.* **3**, 307–310 (2004). <https://doi.org/10.1038/nmat1118>
- [46] Finkelmann, H., Greve, A., Warner, M.: The elastic anisotropy of nematic elastomers. *Eur. Phys. J. E* **5**, 281–293 (2001). <https://doi.org/10.1007/s101890170060>
- [47] Rivlin, R.S.: Large elastic deformations of isotropic materials. I. Fundamental concepts. *Phil. Trans. Roy. Soc. Lond. A* **240**(822), 459–490 (1948)
- [48] Kubo, R.: Large elastic deformation of rubber. *J. Phys. Soc. Japan* **3**, 312–317 (1948)
- [49] Truesdell, C., Noll, W.: *The Non-Linear Field Theories of Mechanics*, 3rd edn. Springer, Berlin (2004). Edited by S.S. Antman
- [50] Treloar, L.R.G.: *The Physics of Rubber Elasticity*, 3rd edn. Oxford Classic

Texts in the Physical Sciences. Oxford University Press, Oxford (2005)

- [51] Deam, R.T., Edwards, S.F.: The theory of rubber elasticity. *Philos. Trans. R. Soc. London A* **280**, 317–353 (1976). <https://doi.org/10.1098/rsta.1976.0001>
- [52] Singh, H., Virga, E.G.: A ribbon model for nematic polymer networks. *J. Elast.* (2022). <https://doi.org/10.1007/s10659-022-09900-9>
- [53] Warner, M.: New elastic behaviour arising from the unusual constitutive relation of nematic solids. *J. Mech. Phys. Solids* **47**, 1355–1377 (1999). [https://doi.org/10.1016/S0022-5096\(98\)00100-8](https://doi.org/10.1016/S0022-5096(98)00100-8)
- [54] van Oosten, C.L., Harris, K.D., Bastiaansen, C.W.M., Broer, D.J.: Glassy photomechanical liquid-crystal network actuators for microscale devices. *Eur. Phys. J. E* **23**, 329–336 (2007). <https://doi.org/10.1140/epje/i2007-10196-1>
- [55] Sonnet, A.M., Virga, E.G.: *Dissipative Ordered Fluids. Theories for Liquid Crystals*. Springer, London (2012)
- [56] Mihai, L.A., Goriely, A.: A plate theory for nematic liquid crystalline solids. *J. Mech. Phys. Solids* **144**, 104101 (2020). <https://doi.org/10.1016/j.jmps.2020.104101>
- [57] Podio-Guidugli, P.: An exact derivation of the thin plate equation. *J. Elast.* **22**, 121–133 (1989)
- [58] Eisenbach, C.D.: Effect of polymer matrix on the cis-trans isomerization of azobenzene residues in bulk polymers. *Makromol. Chem.* **179**, 2489–2506 (1978). <https://doi.org/10.1002/macp.1978.021791014>
- [59] Serra, F., Terentjev, E.M.: Nonlinear dynamics of absorption and photo-bleaching of dyes. *J. Chem. Phys.* **128**, 224510 (2008). <https://doi.org/10.1063/1.2937455>
- [60] Sluckin, T.J., Dunmur, D.A., Stegemeyer, H.: *Crystals that Flow*. Taylor & Francis, London, New York (2004)